

www.acsami.org Research Article

Biomimetic Hierarchies for Universal Surface Enhancement and Applications in Water Treatment

Yifei Liu, Ajit K. Roy, and Donglei Emma Fan*



Cite This: ACS Appl. Mater. Interfaces 2024, 16, 56285-56292



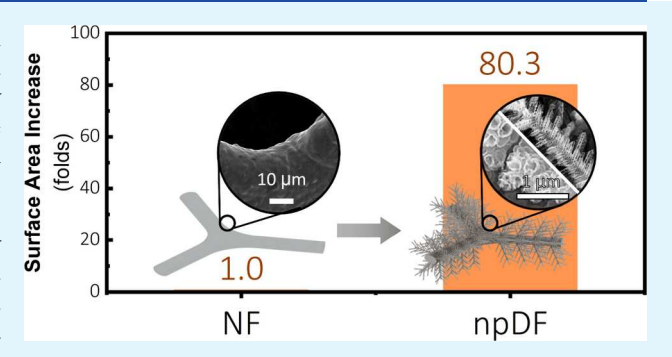
ACCESS I

III Metrics & More

Article Recommendations

s Supporting Information

ABSTRACT: Hierarchical superstructures, ubiquitously found in nature, offer enhanced efficiency in both substance reaction and mass transport owing to their unique multiscale features. Inspired by these natural systems, this research reports a general and scalable electrochemical scheme for creating highly branched, multilevel porous superstructures on various electrically conductive substrates. These structures exhibit cascading features from centimeters, submillimeters, micrometers, down to sub-100 nm, significantly increasing the surface area of substrates, such as foams, foils, and carbon cloth by 2 orders of magnitude—among the highest reported enhancements. This versatile and low-cost method, applicable to a range of electrically conductive substrates, enables innovative flow-



assisted water purification with enhanced energy efficiency. The performance, successfully removing 99% of mercury within 0.5 h at 540 rpm and meeting the U.S. Environmental Protection Agency (EPA) safety standards for drinking water, further validates the advantages of these unique structures. Overall, the reported general, economical, and versatile scheme could broadly impact energy and environmental remediation.

KEYWORDS: biomimicry, hierarchical, nanoporous, electrochemistry, water treatment

■ INTRODUCTION

Basic fluid transfer involves, migration, diffusion, and convection.^{1,2} It is important to harmonize all three processes for an efficient matter exchange system, for either chemical reactions or physical processes.^{3–5} Hierarchical superstructures with feature sizes spanning from micro/nanometers to meters are ubiquitously found in nature.⁶⁻⁸ Such unique structures provide advantages in facilitating rapid substance interaction with surroundings at small scales as well as efficient mass transport at large scales. Life in nature has adopted hierarchical superstructures and leveraged their advantageous properties over millions of years to optimize substance transport, exchange, and reactions with its surroundings. Examples include plant roots, tree crowns, neurons, and vertebrates' lymphatic and cardiovascular systems. 1,9-13 Learning from nature, it is highly desirable to innovate a general and rational approach for introducing multilevel hierarchical structures to interesting man-made substrates or devices to enhance their performances that require large specific surface areas as well as dually high speed in chemical reactions and mass transport. The applications include batteries, supercapacitors, electrocatalysts, and water-purification membranes.

A human lung is an excellent example of a functional hierarchical superstructure. It starts from the trachea, where the conducting airway tree ends in $\sim 30,000$ tufts of gas exchanging air ducts that form the acini. These acini constitute

a complex of six-eight generations of branched alveolar ducts decorated with alveoli and a dense capillary network. The overall structure is 3D hierarchical with multiple scales ranging from the centimeter trachea to the finest alveoli of tens of micrometers, where gas exchange occurs. The unique structure, made of only ~300 g of tissue, enables a remarkable alveolar surface area of 130 m² within a volume of only a few liters. Such a structural arrangement allows instantaneous augmentation of energy needs by a factor of 10 or more when a mammal explodes from a rest pose. 1,14,15 With these insights, various artificial 3D hierarchical porous superstructures have been created for enhancing device performance. For instance, polymer electrolyte fuel cells with lung-inspired flow-field design exhibit enhanced mass transport.4 The same effect is found in hierarchical structures made of ZnO and carbonaceous materials for photocatalysis, electrocatalysis, gas sensing, and Li storage. Recently, the rapid mass transport property inherent in hierarchical structures is also explored in personal cooling management.^{25,26}

Received: June 25, 2024
Revised: September 23, 2024
Accepted: September 24, 2024
Published: October 7, 2024





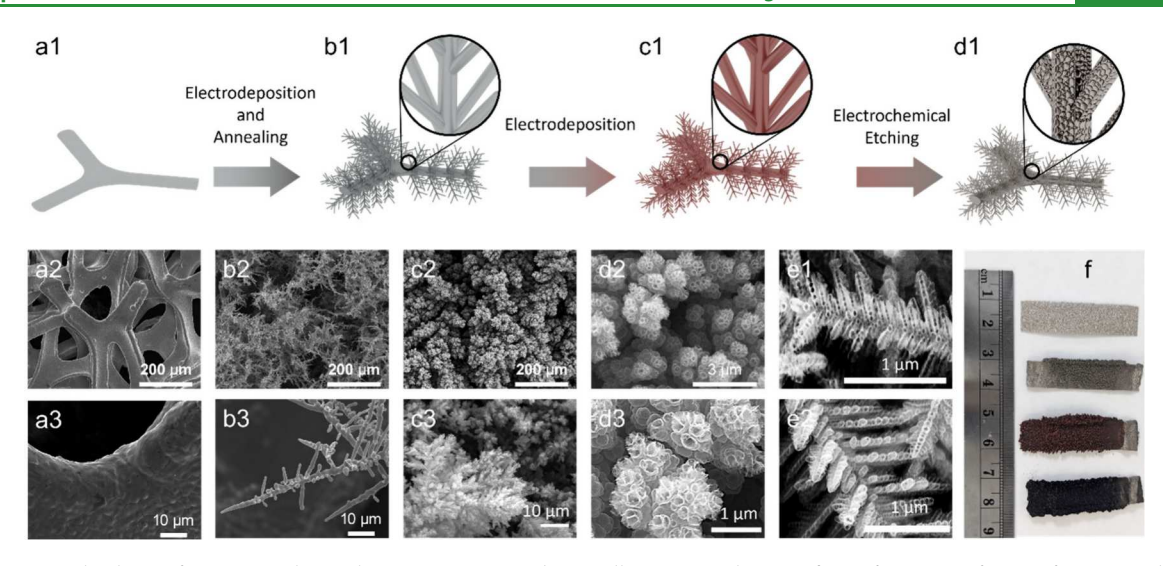


Figure 1. Rational scheme for creating hierarchic structures to substantially increase the specific surface area of a 3D foam via additive and subtractive electrochemistry. (a1–d1) Fabrication flowchart and (a2–d3) corresponding SEM images of (a2, a3) Ni foam; (b2, b3) electrodeposition for adding 3D dense microbranches and annealing; (c2, c3) electrodeposition of phase-separated Cu/Ni films on the highly branched foam; (d2, d3) selective etching of Cu to create nanoporous dendritic foam with hierarchical features at 100 μ m (a1–a3), 10 μ m (b1–b3), and less than 100 nm (e1–e2). (f) Sample photographs at stages of a1–d1.

This far, various fabrication methods have been utilized to create hierarchically porous structures, including templateassisted and template-free methods and postsynthesis treatment.^{27,28} Template-assisted fabrication generally requires a sacrificial structure that is removed after the target porous structures are formed. The employed template varies from surfactant, macroporous polymer, colloidal crystal, emulsion, to biotemplates. ^{29–33} This approach results in excellent control over pore size and structural geometry; however, the fabrication is often complicated and costly. Template-free methods include sol-gel controlling, zeolitization, supercritical fluids, freeze-drying, breath figures, and selective leaching. 34-39 Recently, a new freeze-drying-free and ionic cross-linking method has been reported for synthesizing foams at 200 μ m in pore size. 40 The template-free processes often entail delicate control and stringent conditions and mostly produce porous oxide or polymer superstructures. In contrast, most hierarchically porous metals are made via a template-assisted synthesis or selective dealloying. The dealloying methods often involve costly noble metal alloys, such as Au and Pt. 41-43 To overcome the issues, recently, nickel nanowires have been directly used as building blocks for assembling porous structures, and plasmadry-etching technique directly creates high-purity nanoporous metal foams without dealloying. 44,45 Nevertheless, endowing 3D hierarchically porous superstructures to an arbitrary substate with substantially improved surface areas and reliable performance remains a daunting task. One notable attempt is via micro/nanoparticles attachment to Ni foams with surface area enhancement from 3 to 20 times, 46-48 and another is via alloying and dealloying of Al with a surface improvement of 77 times.

In this research, we report a general, economy, and room temperature approach, all based on manufacture-friendly electrochemical processes, to introduce biomimetic multilevel hierarchies with features ranging from less than 100 nm, tens of micrometers, submillimeters, to centimeters, on a variety of conductive substrates and surfaces. This innovation strategically capitalizes on the advantages of both submillimeter-scale and micro/nanometer-scale structures, where the former

facilitating rapid and efficient transport of bulk fluidic reactants and the latter providing an exceptionally high contact surface for chemical reactions or exchange. Notably, the resulting hierarchical foam exhibits a remarkable increase in specific surface area by 2 orders of magnitude on various surfaces, including metallic foams, foils, and carbon cloth, among the highest enhancements reported so far. For demonstration purposes, the processed foams are applied in flow-assisted water treatment, which readily yield 99% mercury removal, reaching EPA guided drinkable standard of 2 ppb, in 30 min at 540 rpm, substantially improved from that obtained from a stationary foam.

RESULTS AND DISCUSSION

In experiments, the fabrication proceeds following the schematic in Figure 1. Various electrically conductive substrates, including commercial Ni foams, carbon cloth, and Ni foils, have been explored to test the proposed fabrication concept. As an example, we briefly describe the fabrication and optimization procedure using Ni foams as the starting substrates. The commercial Ni foams rolled to 200 μ m in thickness are made of 3D continuously interconnected microstruts with micropores of $\sim 100-200 \ \mu m$ (Figure 1a). After removal of surface oxide in sulfuric acid, large arrays of Ni/Cu microbranches are electrodeposited on the 3D microstructs, filling into the pores and growing out of the surface at -1.4 V (Ag/AgCl, 3 M NaCl) in electrolyte made of Ni²⁺, Cl⁻, SO₄²⁻, and Cu²⁺ (Figures S1 and S2). The highly branched microstructures are dendritic with a cascading hierarchy; the features range from several hundreds of micrometers in the main trunk, tens micrometers in the firstlevel branches, to a few to submicrometers in the secondary branches. The presence of copper and chloride ions play critical roles in the formation of the microbranching structures, which enables rapid growth of Cu in the alloy. 19,50-52 Next, the highly branched foams are annealed at 1000 °C for 5 min, which effectively enhances the adhesion of the microbranches on the Ni foam (Figure 1b). Then, the branched metal dendritic foam (DF) is subjected to the second round of Cu/

Ni electrochemical processing, including both electrodeposition and electroetching, in a different electrolyte made of Ni²⁺, SO_4^{2-} , and Cu^{2+} at -1.0 V (Ag/AgCl electrode, 3 M NaCl). Distinctively, in this process, Cu/Ni films are electrodeposited conformably on the branched Ni foam along with cluster formation, leading to 3D broccoli-like features (Figure 1c). After etching Cu from the electrodeposited Ni/Cu alloy at 0.5 V (Ag/AgCl, 3 M NaCl), we obtain unique three-level nanoporous superstructures made of close-assembled Ni nanopores of largely uniform size arranged into 3D fractal structures (Figure 1d). In this step, Cu can be electroetched selectively from the Ni/Cu alloy, which has an optimized atomic ratio resulting in phase separation during electrodeposition. The passivation of Ni in the electrolyte further assists the selective electroetching of Cu. 53-55 The progress of Cu etching is monitored by the electric current, which decreases rapidly until reaching 14 mA, at which nanopores have been successfully generated (Figures S3 and S4).

Moreover, the hierarchical morphologies of the obtained structures can be readily tailored by the reaction conditions. In the condition mentioned earlier, the structures that are formed mimic the morphology of human lungs, as shown in Figures 1d2 and 1d3. These structures consist of nanoporous spheroidal microclusters that represent the most refined fractal layer, resembling the myriad of micrometer-sized sacs found at the deepest fractal level of the branching trachea. When tuning the reaction conditions, e.g., creating nanopores via electrodeposition at $-1.1~\rm V$ in 0.2 M NiSO4, 0.025 M CuSO4-48C, and etching until 14 mA, the 3D superstructures exhibit a different morphology with ordered arrays of nanopores of $\sim\!40~\rm nm$ distributing along the lengths of long microbranches (Figures 1e1 and 1e2).

This strategic fabrication approach, reproducibly creating highly packed sub-100 nanopores on tens of micrometers long branches growing in quasi-3D on a surface, results in substantial surface-area enhancement. Here we determine the specific surface area with both electrochemical surface area (ECSA) measurements and Brunauer-Emmett-Teller (BET) analysis. The ECSA determines the well-reproducible \sim 80-fold increase of surface area from Ni foam substrates, which agrees with that obtained from the BET surface area analysis (Figure 2a,b). Further analysis shows that the BET surface area of the nanopores conformably coated on the microbranches, 4.59 m²/g (Supporting Note S1), aligns with those of nanoporous metal films with a ligament size of ~ 50 nm at $\sim 3-7$ m²/g. ⁵⁶ Different from previous work, our nanoporous structures are configured in a 3D hierarchical manner, which permits rapid liquid flow transport, as that demonstrated in flow-assisted water treatment. Further characterization of the multilevel superstructures made at different stages indicates that the greatest surface-area enhancement is contributed by the plethora of nanopores made on the supporting branched Ni/ Cu foams, accounting for ~20-fold and ~4-fold total increase, respectively. Importantly, the fabrication scheme is general, which can be easily applied to different conductive substrates, such as Ni foams, carbon cloth, and even Ni foil, resulting in universally increased surface area by 2 orders of magnitude from starting materials (Figure 2c,d).

This remarkable over-80-fold surface-area enhancement has been realized via systematically optimizing the electrodeposition and electroetching process of Ni/Cu films coated on the dendritic foams (Figure 1, step 2). In this step, we methodically modulate two controlling parameters, the

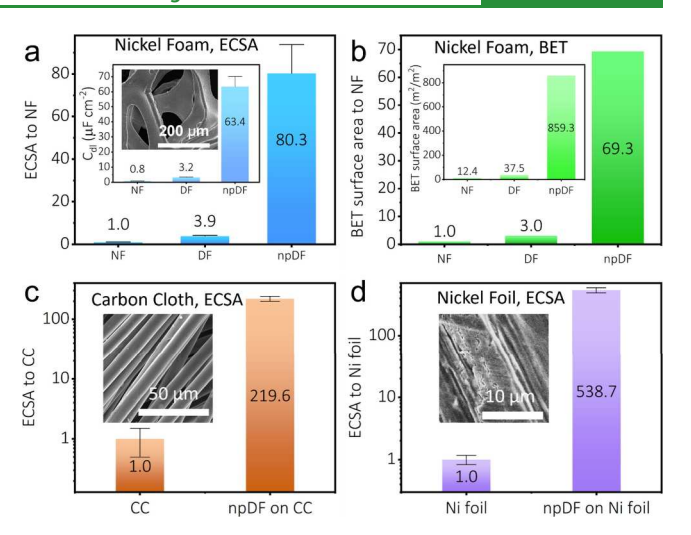


Figure 2. (a, b) Substantial, consistent enhancement of specific surface areas to \sim 70–80 folds on Ni foams confirmed by both (a) ECSA and (b) BET measurements. (a) Inset plot: ECSA measured electric double-layer capacitance per unit area. Inset SEM image: Ni foam. (b) Inset: BET surface area was measured from nickel foams (NF), dendritic nickel foams (DF), and nanoporous dendritic Ni foams (npDF). (c, d) The same approach is readily applicable for surface-area enhancement for various foams and films, such as (c) carbon cloth (SEM image in the inset) and (d) metallic Ni foil (SEM image in the inset). The overall surface-area enhancement reaches 2 orders of magnitude.

concentration of copper ions in electrolyte and total electric charges passing through the circuit, which govern the alloying ratio of the deposited Cu/Ni and its overall amount, respectively. As shown in Figure 3, the ECSA monotonically increases with the amounts of deposited charges when the concentration of copper is controlled between 0.01 and 0.07 M. The enhancement of surface area reaches 77 times at 0.07 M Cu at a total deposition charge of 400-500 C. At 0.01 M, an ultralow Cu ion concentration, the increase of surface area is limited to \sim 30-fold, which can be attributed to the restricted formation of Ni nanopores (Figure S5a,b). On the other side, at the high end of Cu concentration (0.09-0.1 M), nanopore formation is also reduced due to the overly etched Ni/Cu film that limits the enhancement to ~60 times (Figure S5c,d). These results are distinct from those observed at the low-level Cu concentration (0.01-0.03 M), which monotonically increases with the total amount of electric charges going through the circuit. An overall analysis indicates that the optimized surface area enhancement due to pore formation occurs at a Cu concentration above 0.05 M. Interestingly, with the increase of Cu concentration, the optimal electric charges for surface area enhancement monotonically shift toward a lower value, where 500 and 300 C offer the highest surfacearea enhancement for an electrolyte made of 0.05 and 0.09 M Cu ion solutes, respectively (Figure 3a-c). The above experimental findings can be understood qualitatively as discussed in the Supporting Information (Supporting Notes

More importantly, the technique demonstrated in this work is general and has shown its success in enhancing various 3D substates, including carbon cloths (CC) and metallic Ni foils. Employing the optimized electrochemical conditions discussed above, the specific areas can be reproducibly increased by 220-and 538-fold, respectively (Figure 2c,d). Nanoporous hier-

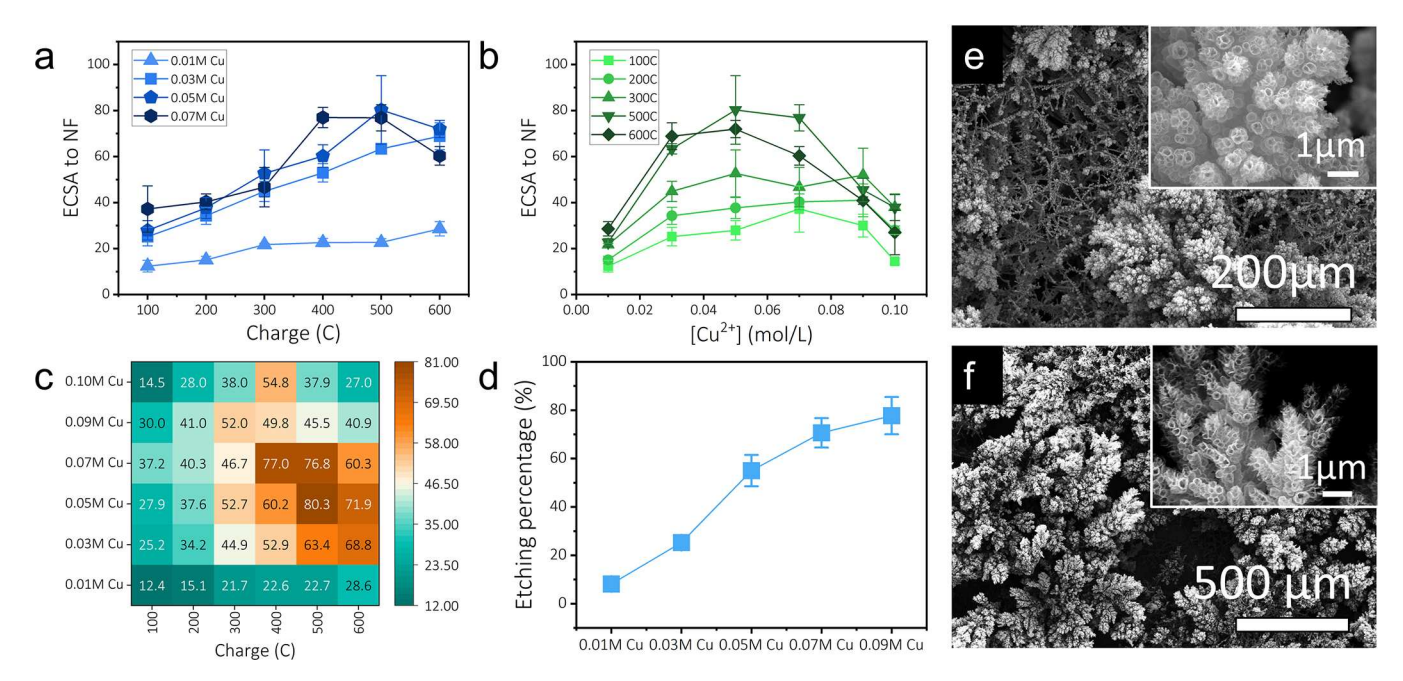


Figure 3. Systematic optimization of surface-area enhancement of Ni foams via electrochemical deposition and subtractive etching. (a) Overall, ECSA surface areas monotonically increase with total deposited charges (100-600 C) at an optimized Cu concentration at 0.01-0.07 M in electrolyte (b) in the range of 0.01-0.1 M. (c) Comprehensive heatmap readily identifies optimized conditions (Cu concentration and total charges) for ECSA surface-area enhancement to \sim 80-fold. (d) Electroetching of Cu enables nanopore formation, the extent of which increases with Cu concentration. (e, f) The same approach has been validated on various conductive substrates, including (e) carbon cloths (f) and Ni foil.

archical structures are successfully added to both types of substrates, with similar features and morphologies to those created on Ni foams, as shown in Figure 3e,f.

The above results demonstrate a new, universal, and effective scheme for enhancing an electrically conductive substrate's surface area by orders of magnitude. The fabrication is facile and economic and all at room temperature. It is intriguing to query if the three-step process in Figure 1 can be simplified. For instance, whether it is feasible to directly grow nanoporous foams via a single combined process of electrodeposition and electroetching of Ni/Cu films in Figure 1c,d without the use of predeposited ramified microbranches (Figure 1b) for substantial surface-area enhancement.

To address the above question, we conducted a series of experiments. It is found that if just using a combined electrochemical process of creating nanopores from Ni/Cu films, it is indeed possible to create a porous structure with semi-freestanding conglomerates grown on a given substrate, such as Ni foams. The ECSA also reaches a level on par with those containing highly branched Ni foams (Figure S6). However, these foams suffer from apparent fragility, which easily shed and break even with ultragentle and careful handling. In comparison, the hierarchical foams made with the intermediate branching step are much more mechanically robust and durable during electroetching, rinsing, and handing, which can be attributed to the 3D structural support from the high-density microbranches annealed to the interconnected microstruts of the Ni foam.

Next, we demonstrate the application of the obtained multilevel nanoporous foams in water remediation by leveraging their unique structurally endowed high-speed flow transport and chemical reactions. With the rapid development of modern industry, heavy metal pollution has become a serious environmental issue. In particular, mercury-contaminated water poses serious health risks. Chronic exposure to

even a low level of mercury can lead to neurological damage and developmental issues in children. It is found that sulfide is a highly effective absorbent for Hg. $^{57-59}$ With this in mind, we first sulfurize the hierarchically porous Ni foams made following the process in Figure 1 via hydrothermal reaction at 120 °C for 6 h (details in the Experimental Section). The resulting foams (npDF_S) maintain the large-scale 3D architecture and hierarchical nanoporous features with sizes ranging from 100 $\mu \rm m$ to 10 $\mu \rm m$ to 100 nm (Figure 4a,b). The structures are also effectively functionalized with Ni₃S₂ after the sulfurization processing as shown in the XRD spectrum (Figure 4c).

We apply such a foam toward high-speed mercury removal from water, where the features of hundreds of micrometers permit rapid water flux through the foam and the high-density 100 nm pores readily provide large interfacial area with water flows for effective mercury absorption. To controllably induce water flow through the foam, it is held stationarily and fully immersed in 14 mL of water in a customized motor-driven rotary cup, which is designed and prototyped using 3D printing as shown in Figure 4d. In a typical experiment, a 1 × 2 cm² npDF_S sample is placed in water with 200 ppb of mercury at the center of the cylindrical rotary cup. Then, the motor drives the water-decontamination device to spin from 180 to 540 rpm, which effectively forces water flowing through the npDF_S hierarchical foam.

Owing to the ultrahigh surface areas, a stationary npDF_S foam can instantly reduce water of 200 ppb Hg to 33 ppb in ~1 s (Figure 4e) and further to 25 ppb in 30 min (Figure 4f). In contrast, sulfurized Ni foams, the substrate of the hierarchical superstructures, can only reduce Hg to 153 ppb after dipping (~1 s), supporting the remarkable surface-area enhancement effect (Figure S7). However, it can be seen that the decontamination speed of the npDF_S foam rapidly decreases with time. To accelerate Hg removal, we leverage the

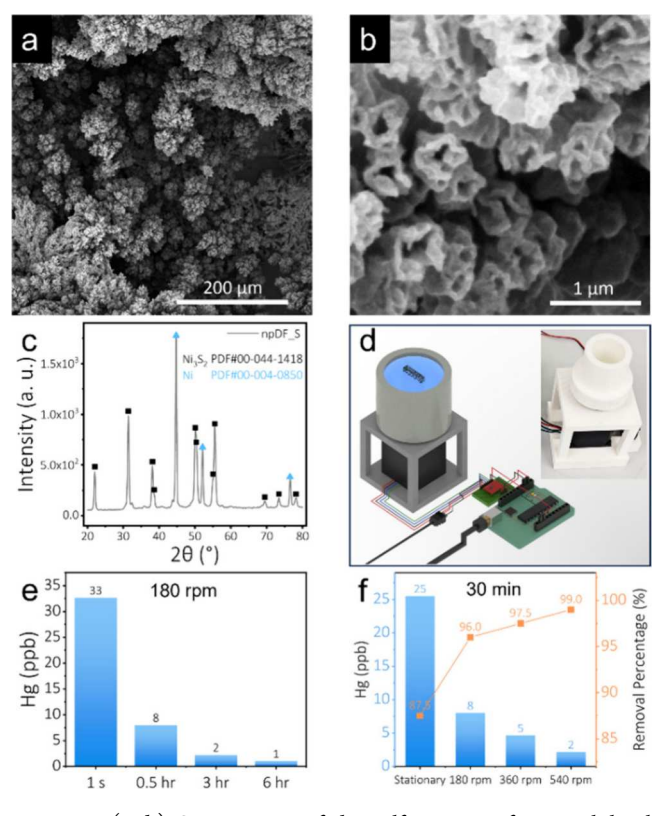


Figure 4. (a, b) SEM images of the sulfurization of 3D multilevel porous Ni results in hierarchical structures with enriched $\mathrm{Ni}_3\mathrm{S}_2$ and (c) X-ray diffraction characterization. (d) The hierarchical structure is integrated into a rotary Hg-removal device, which offers reduced energy consumption and flow-enhanced efficiency in Hg removal. Inset: photo of a 3D-printed device prototype. (e) Hg removal efficiency monotonically increases with (e) operation duration (180 rpm) and (f) device rotation speed (30 min). Hg is successfully removed from water reaching the 2 ppb as safety level set by the EPA of US in 30 min at 540 rpm, in contrast to 3 h needed at 180 rpm.

advantageous multilevel hierarchy of the superstructures and generate flows by rotating the water-treatment cup. It is found that Hg concentration in water monotonically reduces with an increase of rotating speed. At 540 rpm, it only takes 0.5 h to reduce Hg level to 2 ppb (Figure 4f), reaching the drinkable standard recommended by The U.S. Environmental Protection Agency (EPA).⁶⁰ When rotating at a lower speed of 180 rpm, it can take 3 h for reducing Hg to the same level, 2 ppb, and a total of 6 h to reach 1 ppb (Figure 4e), suggesting the important role of water flow for accelerating water decontamination. In comparison, the control sample, sulfurized Ni foam, can only remove 51.4% of Hg to 97 ppb after rotating at 540 rpm for 0.5 h (Figure S7). Moreover, the strategical multilevel structural design not only permits rapid water transport and 3D water-device interactions for flow-enhanced mercury removal but also requires a lower energy consumption, 11% by estimation, compared to those nonhierarchical nanoporous structures (Supporting Note S3, Figures S8 and S9). Indeed, such a design is advantageous in meeting the demand of advanced applications that require both high flow transport and large surface area for enhanced reaction, such as water treatment, electrodes for energy storage, and electrochemical catalysis. After the mercury absorption, approaches are available for regenerating the npDF S substrates. For instance, it has been reported that the reduction-and-volatilization

methods can catalytically reduce Hg^{2+} to Hg^0 in disodium citrate, followed by the volatilization of mercury at 80 °C. 61,62

CONCLUSION

In conclusion, we propose and successfully validate an innovative, rational, and general method for substantially increasing the surface area of a given substrate via creating multilevel-featured superstructures using synergistic additive and subtractive electrochemical processes. Such a structure is inspired by the ubiquitously observed counterpart biological systems, such as lungs of vertebrates containing highly branched airways connecting numerous small alveoli. Akin to their biological counterparts, our strategically created inorganic superstructures with features ranging from 100 μ m to less than 100 nm provide both high mass-transport conductance and large surface-area for rapid chemical reaction, as demonstrated in the multifold flow-flux enhanced water remediation. Such a design is also advantageous in its reduced energy consumption for flow-assisted applications compared to that of a solid structure.

Importantly, the fabrication strategy permits the making of such structures on a variety of electrically conductive substrates, not only on metallic substrates such as Cu and Ni but also on films such as carbon cloth and even metallic foils. The specific surface area can be robustly promoted by 2 orders of magnitude compared to the starting substrates, which is among the highest enhancements reported so far. Overall, this research provides a practically viable, low-cost, and applicable approach for creating hierarchical features and enhancing surface areas. It is expected to broadly impact energy storage devices, electrocatalysis, water treatment, and tissue engineering.

■ EXPERIMENTAL SECTION

Synthesis of High-Density Microbranches on a Conducting Substrate. Sample Preparation. The dendritic foam (DF) was synthesized on an electrically conductive substrate including nickel foams (NF), Ni foils, and carbon cloth (CC). The substate, such as a piece of commercial nickel foam rolled to 200 μm in thickness (NF, 2 \times 4 cm², MTI Corporation, CA, USA, Cat. # EQ-bcnf-16m), was successively cleaned by acetone, sulfuric acid (H₂SO₄, 3 M), and DI water to remove the surface oxide layer. For carbon cloth, it was immersed in 4 M HNO₃ at 60 °C for 4 h to induce hydrophilicity. After rinsing with DI water and dried in air, the material was subjected to the following fabrication steps.

Fabrication Step 1: Growth of Diverging Ni/Cu Microbranches. The Ni/Cu microbranches were electrodeposited at −1.4 V (vs Ag/ AgCl, 3 M NaCl) for 150 C in an electrolyte made of copper sulfate (CuSO₄, 0.0025 M), nickel chloride (NiCl₂, 0.1 M), and boric acid (H₃BO₃, 0.323 M), where nickel foils (Alfa Aesar, Ward Hill, MA) were used as the counter electrodes. The electrodeposition is assisted by magnetic stirring at a speed of 120 rpm and repeated 4 times with the substrate, such as NF, flipped upside-down each time for uniform coverage of the microbranches. The resultant substrate was rinsed with DI water and ethanol and dried overnight in a vacuum dryer. Next, the sample was rapidly annealed for 5 min at 1000 °C in a tube furnace (Lindberg/Blue M Mini-Mite Tube Furnaces, Thermo Scientific) with a flow of mixed hydrogen (H₂, 5 sccm) and nitrogen (N₂, 50 sccm) of about 440 mTorr to improve the mechanical adhesion strength between the ramified microbranches and the foam substrates. After annealing, the highly branched foam was cooled to room temperature and cut into two pieces of 1 × 4 cm² each for

Fabrication Step 2: Large-Scale Creation of a Nanoporous Layer on a Highly Branched Foam. A typical electrolyte for making a highly branched nanoporous dendritic foam (npDF) is 0.4 M NiSO₄,

0.65 M H₃BO₃, and 0.05 M CuSO₄. The concentration of CuSO₄ was varied to optimize the resulting product, ranging from 0.01 to 0.10 M. The electrodeposition was carried out at -1.0 V (vs Ag/AgCl, 3 M NaCl), with charges changing from -100 to -600 C in a 3-electrode configuration. Because the actual immersed area of the foam is only 1 \times 3 cm² (1 \times 1 cm² is above the surface of the electrolyte), the corresponding deposition charge density is 16.7–100 C/cm² with the consideration of the double-sided deposition. A piece of Ni foil worked as the counter electrode. Once the electrodeposition was accomplished, electrochemical etching was performed at 0.5 V (vs Ag/AgCl, 3 M NaCl) until the electric current was reduced to <14 mA. At this current density, it was found that the etching process became extremely slow, indicating that Cu was mostly removed. Next, the npDFs were rinsed by DI water for at least 1 min to remove any remaining electrolyte and dried in air.

Hydrothermal Sulfurization of NpDF_S and NF_S. The obtained npDF or Ni foam (NF) was immersed into a 50 mL autoclave containing a mixture of 35 mL of DI water and 0.6 g of thiourea followed by autoclaving at 120 °C for 6 h. After the hydrothermal reaction, the npDF S or NF S was taken out after the solution is cooled to room temperature and rinsed by DI water carefully for 1 min before dried in air.

Demonstration for Water Decontamination. The npDF S was trimmed into a piece of 1 × 2 cm². Then it was attached to a platinum foil via a Kapton-tape-covered binder clip. Then this combination was set on a rack on top of the water treatment prototype and fully immersed in a Hg-contaminated water sample. The cylindrical water treatment prototype can be readily rotated and controlled by a programmable motor under it. The rotation readily forced the water body to pass through the hierarchical structures of the npDF S. The rotating speed was controlled to 180, 360, and 540 rpm.

Electrochemical Surface Area Tests. The electrochemical surface area tests were carried out in a three-electrode cell setup in potassium hydroxide solution (1 M KOH, aq); a carbon rod served as the counter electrode, and Hg/HgO (1 M NaOH, aq) served as the reference electrode.

ASSOCIATED CONTENT

Supporting Information

The Supporting Information is available free of charge at https://pubs.acs.org/doi/10.1021/acsami.4c10548.

> Calculation of the BET surface area of nanopores, discussion of the optimization of the formation of the nanopores, and simulation results of the energy consumption for plate substrate and porous substrate; figures of SEM images, cyclic voltammogram, and chronoamperometry (PDF)

AUTHOR INFORMATION

Corresponding Author

Donglei Emma Fan - Materials Science and Engineering Program, Texas Materials Institute, The University of Texas at Austin, Austin, Texas 78712, United States; Walker Department of Mechanical Engineering and Chandra Department of Electrical and Computer Engineering, The University of Texas at Austin, Austin, Texas 78712, United States; o orcid.org/0000-0002-4724-2483; Email: dfan@ austin.utexas.edu

Authors

Yifei Liu – Materials Science and Engineering Program, Texas Materials Institute, The University of Texas at Austin, Austin, Texas 78712, United States; orcid.org/0000-0003-0247-1247

Ajit K. Roy - Air Force Research Laboratory, Materials and Manufacturing, Dayton, Ohio 45402, United States; orcid.org/0000-0002-3344-7437

Complete contact information is available at: https://pubs.acs.org/10.1021/acsami.4c10548

Notes

The authors declare no competing financial interest.

ACKNOWLEDGMENTS

The authors are grateful for support from Welch Foundation (F-1734) and National Science Foundation (grant #1563382). This research also received support from the National Science Foundation grant #1930649 via INTERN project and National Institutes of Health grant #1R43ES037145-01 in part.

REFERENCES

- (1) Hsia, C. C. W.; Hyde, D. M.; Weibel, E. R. Lung Structure and the Intrinsic Challenges of Gas Exchange. Comprehensive Physiology 2016, 6, 827-895.
- (2) Bard, A. J.; Faulkner, L. R.; White, H. S. Electrochemical Methods: Fundamentals and Applications; John Wiley & Sons: 2001.
- (3) Trogadas, P.; Ramani, V.; Strasser, P.; Fuller, T. F.; Coppens, M.-O. Hierarchically Structured Nanomaterials for Electrochemical Energy Conversion. Angew. Chem., Int. Ed. 2016, 55 (1), 122-148.
- (4) Trogadas, P.; Cho, J. I. S.; Neville, T. P.; Marquis, J.; Wu, B.; Brett, D. J. L.; Coppens, M.-O. A Lung-Inspired Approach to Scalable and Robust Fuel Cell Design. Energy Environ. Sci. 2018, 11 (1), 136-
- (5) García-López, I.; Arenas, L. F.; Turek, T.; Agueda, V. I.; Garrido-Escudero, A. Mass Transfer Enhancement in Electrochemical Flow Cells through 3D-Printed Biomimetic Channels. React. Chem. Eng. **2023**, 8 (7), 1776–1784.
- (6) Fratzl, P.; Weinkamer, R. Nature's Hierarchical Materials. Prog. Mater. Sci. 2007, 52 (8), 1263-1334.
- (7) Chen, Q.; Pugno, N. M. Bio-Mimetic Mechanisms of Natural Hierarchical Materials: A Review. J. Mech. Behav. Biomed. Mater. 2013, 19, 3-33.
- (8) Tseng, P.; Napier, B.; Zhao, S.; Mitropoulos, A. N.; Applegate, M. B.; Marelli, B.; Kaplan, D. L.; Omenetto, F. G. Directed Assembly of Bio-Inspired Hierarchical Materials with Controlled Nanofibrillar Architectures. Nat. Nanotechnol. 2017, 12 (5), 474-480.
- (9) Weibel, E. R.; Sapoval, B.; Filoche, M. Design of Peripheral Airways for Efficient Gas Exchange. Respir. Physiol. Neurobiol. 2005, 148 (1), 3-21.
- (10) Hsia, C. C. W.; Hyde, D. M.; Ochs, M.; Weibel, E. R. An Official Research Policy Statement of the American Thoracic Society/ European Respiratory Society: Standards for Quantitative Assessment of Lung Structure. Am. J. Respir. Crit. Care Med. 2010, 181 (4), 394-
- (11) Weibel, E. R. Fractal Geometry: A Design Principle for Living Organisms. Am. J. Physiol.-Lung Cell. Mol. Physiol. 1991, 261 (6), L361-L369.
- (12) Coppens, M.-O. A Nature-Inspired Approach to Reactor and Catalysis Engineering. Curr. Opin. Chem. Eng. 2012, 1 (3), 281–289. (13) Zeide, B. Fractal Geometry in Forestry Applications. For. Ecol. Manag. 1991, 46 (3), 179-188.
- (14) Hakim, A.; Usmani, O. S. Structure of the Lower Respiratory Tract. In Reference Module in Biomedical Sciences; Elsevier: 2014.
- (15) Ochs, M.; Nyengaard, J. R.; Jung, A.; Knudsen, L.; Voigt, M.; Wahlers, T.; Richter, J.; Gundersen, H. J. G. The Number of Alveoli in the Human Lung. Am. J. Respir. Crit. Care Med. 2004, 169 (1),
- (16) Yu, J. G.; Su, Y. R.; Cheng, B. Template-Free Fabrication and Enhanced Photocatalytic Activity of Hierarchical Macro-/Mesoporous Titania. Adv. Funct. Mater. 2007, 17 (12), 1984–1990.

- (17) Doherty, C. M.; Caruso, R. A.; Smarsly, B. M.; Drummond, C. J. Colloidal Crystal Templating to Produce Hierarchically Porous LiFePO4 Electrode Materials for High Power Lithium Ion Batteries. *Chem. Mater.* **2009**, *21* (13), 2895–2903.
- (18) Mai, L.-Q.; Yang, F.; Zhao, Y.-L.; Xu, X.; Xu, L.; Luo, Y.-Z. Hierarchical MnMoO4/CoMoO4 Heterostructured Nanowires with Enhanced Supercapacitor Performance. *Nat. Commun.* **2011**, 2 (1), 381.
- (19) Li, W.; Tekell, M. C.; Liu, C.; Hethcock, J. A.; Fan, D. Flexible All-Solid-State Supercapacitors of High Areal Capacitance Enabled by Porous Graphite Foams with Diverging Microtubes. *Adv. Funct. Mater.* **2018**, 28 (29), 1800601.
- (20) Guo, J.; Chan, A.; Li, W.; Fan, D. L. Kirkendall Effect in Creating Three-Dimensional Metal Catalysts for Hierarchically Porous Ultrathin Graphite with Unique Properties. *Chem. Mater.* **2017**, 29 (11), 4991–4998.
- (21) Zheng, X.; Shen, G.; Wang, C.; Li, Y.; Dunphy, D.; Hasan, T.; Brinker, C. J.; Su, B.-L. Bio-Inspired Murray Materials for Mass Transfer and Activity. *Nat. Commun.* **2017**, *8* (1), 14921.
- (22) Liu, Y.; Li, W.; Ma, Y.; Fan, D. Core-Shell Dendritic Superstructural Catalysts by Design for Highly Efficient and Stable Electrochemical Oxygen Evolution Reaction. *Adv. Mater. Interfaces* **2020**, *7* (16), 2000777.
- (23) Liu, C.; Xu, X.; Rettie, A. J. E.; Mullins, C. B.; Fan, D. L. One-Step Waferscale Synthesis of 3-D ZnO Nanosuperstructures by Designed Catalysts for Substantial Improvement of Solar Water Oxidation Efficiency. *J. Mater. Chem. A* **2013**, *1* (28), 8111–8117.
- (24) Li, W.; Huang, Y.; Liu, Y.; Tekell, M. C.; Fan, D. (Emma). Three Dimensional Nanosuperstructures Made of Two-Dimensional Materials by Design: Synthesis, Properties, and Applications. *Nano Today* **2019**, 29, 100799.
- (25) Miao, D.; Wang, X.; Yu, J.; Ding, B. A Biomimetic Transpiration Textile for Highly Efficient Personal Drying and Cooling. *Adv. Funct. Mater.* **2021**, *31* (14), 2008705.
- (26) Wang, X.; Huang, Z.; Miao, D.; Zhao, J.; Yu, J.; Ding, B. Biomimetic Fibrous Murray Membranes with Ultrafast Water Transport and Evaporation for Smart Moisture-Wicking Fabrics. *ACS Nano* **2018**, *13* (2), 1060–1070.
- (27) Yang, X.-Y.; Chen, L.-H.; Li, Y.; Rooke, J. C.; Sanchez, C.; Su, B.-L. Hierarchically Porous Materials: Synthesis Strategies and Structure Design. *Chem. Soc. Rev.* **2017**, *46* (2), 481–558.
- (28) Li, X.; Yu, J.; Jaroniec, M. Hierarchical Photocatalysts. *Chem. Soc. Rev.* **2016**, 45 (9), 2603–2636.
- (29) Attard, G. S.; Glyde, J. C.; Göltner, C. G. Liquid-Crystalline Phases as Templates for the Synthesis of Mesoporous Silica. *Nature* **1995**, *378* (6555), 366–368.
- (30) Schattka, J. H.; Shchukin, D. G.; Jia, J.; Antonietti, M.; Caruso, R. A. Photocatalytic Activities of Porous Titania and Titania/Zirconia Structures Formed by Using a Polymer Gel Templating Technique. *Chem. Mater.* **2002**, *14* (12), 5103–5108.
- (31) Sadakane, M.; Horiuchi, T.; Kato, N.; Takahashi, C.; Ueda, W. Facile Preparation of Three-Dimensionally Ordered Macroporous Alumina, Iron Oxide, Chromium Oxide, Manganese Oxide, and Their Mixed-Metal Oxides with High Porosity. *Chem. Mater.* **2007**, *19* (23), 5779–5785.
- (32) Zhang, H.; Cooper, A. I. Synthesis and Applications of Emulsion-Templated Porous Materials. *Soft Matter* **2005**, *1* (2), 107–113
- (33) Jia, Y.; Han, W.; Xiong, G.; Yang, W. Layer-by-Layer Assembly of TiO₂ Colloids onto Diatomite to Build Hierarchical Porous Materials. *J. Colloid Interface Sci.* **2008**, 323 (2), 326–331.
- (34) Flaig, S.; Akbarzadeh, J.; Peterlik, H.; Hüsing, N. Hierarchically Organized Silica Monoliths: Influence of Different Acids on Macroand Mesoporous Formation. *J. Sol-Gel Sci. Technol.* **2015**, 73 (1), 103–111.
- (35) Li, C.; Cho, H. J.; Wang, Z.; Gou, J.; Ren, Y.; Xi, H.; Fan, W. Effects of the Framework and Mesoporosity on the Catalytic Activity of Hierarchical Zeolite Catalysts in Benzyl Alcohol Conversion. *ChemCatChem* **2016**, *8* (14), 2406–2414.

- (36) Butler, R.; Hopkinson, I.; Cooper, A. I. Synthesis of Porous Emulsion-Templated Polymers Using High Internal Phase CO₂-in-Water Emulsions. *J. Am. Chem. Soc.* **2003**, *125* (47), 14473–14481.
- (37) Fukasawa, T.; Ando, M.; Ohji, T.; Kanzaki, S. Synthesis of Porous Ceramics with Complex Pore Structure by Freeze-Dry Processing. *J. Am. Ceram. Soc.* **2001**, *84* (1), 230–232.
- (38) Srinivasarao, M.; Collings, D.; Philips, A.; Patel, S. Three-Dimensionally Ordered Array of Air Bubbles in a Polymer Film. *Science* **2001**, 292 (5514), 79–83.
- (39) Kim, H.; da Rosa, C.; Boaro, M.; Vohs, J. M.; Gorte, R. J. Fabrication of Highly Porous Yttria-Stabilized Zirconia by Acid Leaching Nickel from a Nickel-Yttria-Stabilized Zirconia Cermet. *J. Am. Ceram. Soc.* **2002**, *85* (6), 1473–1476.
- (40) Chen, C.; Zhou, Y.; Xie, W.; Meng, T.; Zhao, X.; Pang, Z.; Chen, Q.; Liu, D.; Wang, R.; Yang, V.; Zhang, H.; Xie, H.; Leiste, U. H.; Fourney, W. L.; He, S.; Cai, Z.; Ma, Z.; Li, T.; Hu, L. Lightweight, Thermally Insulating, Fire-Proof Graphite-Cellulose Foam. *Adv. Funct. Mater.* 2023, 33 (6), 2204219.
- (41) Ying, J.; Lenaerts, S.; Symes, M. D.; Yang, X.-Y. Hierarchical Design in Nanoporous Metals. *Adv. Sci.* **2022**, 9 (27), 2106117.
- (42) Ding, Y.; Erlebacher, J. Nanoporous Metals with Controlled Multimodal Pore Size Distribution. *J. Am. Chem. Soc.* **2003**, *125* (26), 7772–7773.
- (43) Xu, C.; Li, Q.; Liu, Y.; Wang, J.; Geng, H. Hierarchical Nanoporous PtFe Alloy with Multimodal Size Distributions and Its Catalytic Performance toward Methanol Electrooxidation. *Langmuir* **2012**, 28 (3), 1886–1892.
- (44) Malloy, J.; Quintana, A.; Jensen, C. J.; Liu, K. Efficient and Robust Metallic Nanowire Foams for Deep Submicrometer Particulate Filtration. *Nano Lett.* **2021**, *21* (7), 2968–2974.
- (45) Kwon, H.; Barad, H.-N.; Silva Olaya, A. R.; Alarcón-Correa, M.; Hahn, K.; Richter, G.; Wittstock, G.; Fischer, P. Dry Synthesis of Pure and Ultrathin Nanoporous Metallic Films. *ACS Appl. Mater. Interfaces* **2023**, *15* (4), 5620–5627.
- (46) Li, H.; Wang, X.; Wang, T.; Xiao, F. A Facile, Green and Time-Saving Method to Prepare Partially Crystalline NiFe Layered Double Hydroxide Nanosheets on Nickel Foam for Superior OER Catalysis. *J. Alloys Compd.* **2020**, 844, 156224.
- (47) Ma, L.; Wei, Z.; Zhao, C.; Meng, X.; Zhang, H.; Song, M.; Wang, Y.; Li, B.; Huang, X.; Xu, C.; Feng, M.; He, P.; Jia, D.; Zhou, Y.; Duan, X. Hierarchical Superhydrophilic/Superaerophobic 3D Porous Trimetallic (Fe, Co, Ni) Spinel/Carbon/Nickel Foam for Boosting Oxygen Evolution Reaction. *Appl. Catal. B Environ.* 2023, 332, 122717.
- (48) Xiong, K.; Li, L.; Zhang, L.; Ding, W.; Peng, L.; Wang, Y.; Chen, S.; Tan, S.; Wei, Z. Ni-Doped Mo 2 C Nanowires Supported on Ni Foam as a Binder-Free Electrode for Enhancing the Hydrogen Evolution Performance. *J. Mater. Chem. A* **2015**, 3 (5), 1863–1867.
- (49) Lee, Y.-J.; Lee, Y.-S.; Shin, H. A.; Jo, Y. S.; Jeong, H.; Sohn, H.; Yoon, C. W.; Kim, Y.; Kim, K.-B.; Nam, S. W. Surface Area Enhancement of Nickel Foam by Low-Temperature Chemical Alloying/Dealloying and Its Application for Sodium Borohydride Hydrolysis. *J. Alloys Compd.* **2020**, 843, 155759.
- (50) Eugénio, S.; Silva, T. M.; Carmezim, M. J.; Duarte, R. G.; Montemor, M. F. Electrodeposition and Characterization of Nickel-Copper Metallic Foams for Application as Electrodes for Supercapacitors. *J. Appl. Electrochem.* **2014**, *44* (4), 455–465.
- (51) Shao, W.; Pattanaik, G.; Zangari, G. Influence of Chloride Anions on the Mechanism of Copper Electrodeposition from Acidic Sulfate Electrolytes. *J. Electrochem. Soc.* 2007, 154 (4), D201.
- (52) Trivedi, R.; Kurz, W. Dendritic Growth. Int. Mater. Rev. 1994, 39 (2), 49-74.
- (53) Sun, L.; Chien, C.-L.; Searson, P. C. Fabrication of Nanoporous Nickel by Electrochemical Dealloying. *Chem. Mater.* **2004**, *16* (16), 3125–3129.
- (54) Chang, J.-K.; Hsu, S.-H.; Sun, I.-W.; Tsai, W.-T. Formation of Nanoporous Nickel by Selective Anodic Etching of the Nobler Copper Component from Electrodeposited Nickel-Copper Alloys. *J. Phys. Chem. C* **2008**, *112* (5), 1371–1376.

- (55) Menezes, S.; Anderson, D. P. Wavelength-Property Correlation in Electrodeposited Ultrastructured Cu-Ni Multilayers. *J. Electrochem. Soc.* **1990**, *137* (2), 440.
- (56) Scandura, G.; Kumari, P.; Palmisano, G.; Karanikolos, G. N.; Orwa, J.; Dumée, L. F. Nanoporous Dealloyed Metal Materials Processing and Applications A Review. *Ind. Eng. Chem. Res.* **2023**, *62* (4), 1736–1763.
- (57) Han, Y.; Tao, J.; Khan, A.; Khan, A.; Ali, N.; Malik, S.; Yu, C.; Yang, Y.; Jesionowski, T.; Bilal, M. Development of Reusable Chitosan-Supported Nickel Sulfide Microspheres for Environmentally Friendlier and Efficient Bio-Sorptive Decontamination of Mercury Toxicant. *Environ. Sci. Pollut. Res.* **2023**, 30 (16), 47077–47089.
- (58) Hsu, C.-J.; Xiao, Y.-Z.; Chung, A.; Hsi, H.-C. Novel Applications of Vacuum Distillation for Heavy Metals Removal from Wastewater, Copper Nitrate Hydroxide Recovery, and Copper Sulfide Impregnated Activated Carbon Synthesis for Gaseous Mercury Adsorption. Sci. Total Environ. 2023, 855, 158870.
- (59) Esmaeili Bidhendi, M.; Parandi, E.; Mahmoudi Meymand, M.; Sereshti, H.; Rashidi Nodeh, H.; Joo, S.-W.; Vasseghian, Y.; Mahmoudi Khatir, N.; Rezania, S. Removal of Lead Ions from Wastewater Using Magnesium Sulfide Nanoparticles Caged Alginate Microbeads. *Environ. Res.* 2023, 216, 114416.
- (60) US EPA, O. National Primary Drinking Water Regulations. https://www.epa.gov/ground-water-and-drinking-water/national-primary-drinking-water-regulations (accessed 2023-10-18).
- (61) Zhi, L.; Zuo, W.; Chen, F.; Wang, B. 3D MoS2 Composition Aerogels as Chemosensors and Adsorbents for Colorimetric Detection and High-Capacity Adsorption of Hg2+. *ACS Sustain. Chem. Eng.* **2016**, *4* (6), 3398–3408.
- (62) Zhang, S.; Li, H.; Wang, Z.; Liu, J.; Zhang, H.; Wang, B.; Yang, Z. A Strongly Coupled Au/Fe₃O₄/GO Hybrid Material with Enhanced Nanozyme Activity for Highly Sensitive Colorimetric Detection, and Rapid and Efficient Removal of Hg2+ in Aqueous Solutions. *Nanoscale* **2015**, *7* (18), 8495–8502.